PHYSICAL REVIEW B VOLUME 51, NUMBER 16 15 APRIL 1995-II

Fractal character of cold-deposited silver films determined by low-temperature scanning tunneling microscopy

Constantine Douketis, Zhouhang Wang, Tom L. Haslett, and Martin Moskovits
Department of Chemistry, University of Toronto and Ontario Laser and Lightwave Research Centre, Toronto, Ontario, Canada M5S 1A1

(Received 25 October 1994; revised manuscript received 19 January 1995)

High-resolution scanning-tunneling-microscope (STM) topographic images of vacuum-deposited Ag films are reported. Films were formed and imaged at 100 and 300 K. Images of films deposited at 300 K, annealed to 560 K, and then returned to 300 K are also presented. The topographic surfaces of the low-temperature films are found to be self-affine fractals with a local Hausdorff-Besicovitch dimension $D = 2.5$. The low-temperature films exhibit intense surface-enhanced Raman spectra (SERS). Films deposited at 300 K do not possess significant fractal character and are not SERS active. We show that the apparent local fractal dimension obtained by analyzing STM topographic images depends critically on the algorithm used. Three such methods (cube counting, triangulation, and power spectrum analysis) are assessed. A method is proposed for obtaining reliable fractal dimensions by analyzing the experimental STM topographic images using several algorithms and comparing the results to a calibration curve generated by applying the same algorithms to simulated fractal surfaces of known Hausdorff-Besicovitch dimension.

INTRODUCTION

Since the discovery of surface-enhanced Raman scattering (SERS) from pyridine adsorbed onto electrochemically roughened Ag (Ref. 1) there has been continued interest in the optical properties of these and other structurally inhomogeneous metal surfaces.[2] Specifically, metal films produced by metal vapor condensation onto very cold surfaces have been the subject of some discussion. While it is universally conceded that cold-deposited films are disordered due to the restricted mobility of the atoms landing on the low-temperature surfaces, there is some controversy regarding the specific morphology of these surfaces. Albano *et al.* suggested that these surfaces consist of many rather flat grains separated by narrow intergrain regions.[3] It was proposed that these intergrain regions are the areas of large electromagnetic enhancement and that only molecules localized in those intergrain regions benefit from the enhancement. The evidence for such a model has been discussed previously and need not be repeated here. There is also an early scanning-tunneling-microscope (STM) study related to cold-deposited films that purports to support this structural model of cold-deposited surfaces.[4] Unfortunately, those images were recorded from cold-deposited films that had been annealed to room temperature. Consequently, it was not possible to surmise their original structure with confidence.

The alternative view of these rough surfaces is given by Bales *et al.*, albeit indirectly.[5] Sputtered films of refractory metals, deposited at room temperature, should display some of the characteristics of cold-deposited films provided the melting temperature of the metal is high enough. Such films have been investigated quite thoroughly. Briefly, they are randomly rough self-affine objects of two limiting types. If the metal vapor source is well collimated so that the atoms approach the substrate, more or less normal to the receiving surface, then in the limit of ballistic aggregation, the film will have a randomly rough interface with an rms roughness height equal to the square root of the mean film thickness. If the source is not well collimated then the films will be coral-like with cavities produced by the coalescence of growing features as a result of the fact that, for any random initial condition of the surface, large surface features will shadow small ones from obliquely incident atoms. These descriptions are limiting cases when no atomic mobility is possible; the situation is commensurately more complicated when this condition is not perfectly achieved.

Large enhancements have been observed for other optical effects in addition to SERS including nonlinear photoemission from rough Ag.[6] The origin of the enhancement involves the excitation of localized dipolar surface plasmons resulting in very intense near-zone fields.[2] Although, in principle, it is possible to solve for the optical response of the system if sufficient structural detail is known, this is in general exceedingly difficult. Moreover, a detailed determination of the structure of the surface is limited by the resolution restrictions of the physical method used.

Recently a theoretical approach has been introduced that can predict some of the gross features of the optical response of rough metal films provided the film is fractal.[7] In that limit, expressions for some physical properties may be deduced in closed form. This theory has been successfully applied to explain degenerate four-wave mixing in fractal colloids where fractality was determined by imaging the distribution of the particles that comprise the colloid.[8] More recently it has been used to explain the enhancement of two-photon electron emission from rough Ag films.[9]

Evidence for fractal character in cold-deposited, rough

0163-1829/95/51(16)/11022(10)/$06.00

Ag films has been reported in experiments involving x-ray reflectivity and adsorption isotherm measurements,[10] but not by direct imaging of the surface morphology using STM. Use of STM as a means of determining fractality has been considered and has been applied to relatively smooth fatigue fracture and sputter-deposited surfaces.[11] STM has been used to examine surface roughness of SERS-active Ag surfaces in electrochemical systems, but in that study fractality was not an issue.[12] STM studies that had searched specifically for fractal character have been conducted on smooth, vacuum-deposited Au films,[13] on electrochemically roughened Au deposits,[14] and on ion-bombarded Fe films.[15]

Cold-deposited, SERS-active metal films have not been explored by STM mainly due to the experimental difficulties of performing high-resolution STM measurements at the low temperatures necessary to maintain SERS activity. Here we confirm the fractal character of these cold-deposited films. In performing the analysis we find that the value of the fractal dimension determined depends critically on the method used to obtain it. In order to circumvent this difficulty we develop a strategy for obtaining fractal dimensions reliably from STM images of, necessarily, limited resolution.

EXPERIMENT

Ag films were explored with a low-temperature, ultrahigh vacuum STM designed and built in-house and briefly described previously.[16] Tungsten tips are attached to a piezoelectric tube scanner. This in turn is attached to a long-range, piezobased drive (Burleigh). The entire drive assembly is mounted on the uppermost of three stages, each vibrationally isolated from the one below it with Viton o-ring loops. The sample substrate is rigidly attached to the upper stage, but with poor thermal contact using Pyrex glass rod and ball junction points. On the other hand, the substrate is in good thermal contact with the bottom of a double cryogenic fluid Dewar through a pair of flexible Cu ribbons. The sample substrate consists of a Cu block (oxygen-free high-conductivity copper) mechanically polished to a mirror finish with 250 nm grit diamond paste.

The ultrahigh vacuum chamber is pumped by a Ti-sublimation pump backed by a turbomolecular pump. The turbomolecular pump can be isolated and shut down during tunneling operation. The base pressure in the apparatus is 2×10^{-11} Torr; this drops by a factor of 2–3 during low-temperature tunneling operation due to cryopumping by the cryostat. With $N_2(l)$ used as the cryogenic fluid, the lowest sample temperature achievable is 100 K (23 K with He(l)]. However, the temperature gradient is stable: single-atom resolution is easily and reproducibly obtainable (highly oriented pyrolytic graphite, single-atom steps in Ag films). The sample reaches thermal equilibrium within 2 h and its temperature is monitored with a thermocouple (0.07% Fe/Au-Chromel). One particularly useful feature of the apparatus is that the sample can be rotated using a worm-gear drive mechanism externally actuated with a fog decoupler. This allows one to rotate the sample away from the tunneling tip, prepare or modify a surface, and then rotate it back so that the tunneling tip axis is again collinear with the surface normal. The sample can also be heated resistively to 600 K. The STM assembly and the walls of the chamber and cryostat are highly polished for low thermal emissivity in order to minimize the thermal load on the microscope. The entire apparatus rests on a massive stone block vibrationally isolated from the floor with air suspension footings.

STM images were recorded in constant current feedback mode at a tunneling current of 1 nA. The tip was biased at -500 mV, resulting in electron flow from the tip to the sample. This current was processed with commercial electronics and software (RHK Tech.). A preamplifier with amplification 10^8 V A^{-1} was used for *I-V* conversion. The Fourier coefficients at all frequencies of noise images were about four orders of magnitude less than topographic image coefficients.

Ag surfaces were prepared by vacuum deposition from an effusive atom source (Ta boat containing 99.999% Ag) at normal incidence and at a film thickness deposition rate of 1 nm s^{-1}. During deposition times of 300 s the pressure in the apparatus typically increased to about 5×10^{-10} Torr. Three types of Ag surfaces were studied: (a) surfaces deposited at 100 K and imaged at 100 K are designated *rough*; (b) surfaces deposited and imaged at 300 K will be referred to as *smooth*; (c) surfaces deposited at 300 K, annealed at 560 K for 5 h, and returned to 300 K for imaging will be termed *annealed smooth.*

Rough Ag surfaces were checked for SERS activity immediately after preparation. The sample was exposed to 0.1–10 L of benzene or ethylene (dose corrected for ion gauge response[17]). Radiation at 488 nm from an Ar$^+$ laser was focused onto the sample with a 25 cm focal length, diffraction limited lens. The laser light was *s* polarized and irradiated the surface with 100 mW of power. Scattered light was collected with a fast internal lens (*f* number 0.8) and directed to a double monochromator (SPEX) outfitted with a single-photon-counting detection system.

FRACTAL ANALYSIS

Real surfaces have been treated as fractal objects by a number of authors.[18] Several caveats must be stated (some have already been expressed in the literature) before proceeding with the fractal analysis of our STM images. (i) The fractal dimension determined for a surface is the *local* Hausdorff-Besicovitch dimension D: it is possible that D is not uniquely defined for a given film and may vary from location to location on the surface. (ii) The STM image of the surface is at most self-affine and not self-similar. This is because the STM height profile is generally much smaller than the scan domain in the plane of the surface and it is necessarily a single-valued function (topographic image) so that overhangs and interfolds of the surface cannot be imaged. (Of course, the film itself may be inherently self-affine.) (iii) Although it is preferable to determine D using data that span many orders of magnitude, thereby demonstrating that the structure scales over a large size range, this is difficult to achieve with current STM instrumental, digitizing, and data handling technology. Typical STM images consist of $(256)^2$ pixels. In order to avoid spurious digital effects it is necessary to reject points that are close to the lower (single pixel) and the upper (full image) size limits. This effectively restricts the scaling region to approximately one order of magnitude, which is normally insufficient to demonstrate fractality confidently. Moreover, the fractal dimension extracted from such restricted data sets have been shown to be suspect. Mitchell and Bonnell concluded that a minimum of $(1024)^2$ pixels were required in order to extract reliable fractal dimensions from STM images.[11] This conclusion was based on the analysis of specific data rather than on a mathematical proof. It remains to be shown whether this conclusion is either general or sufficient. Finally, (iv) the finite size of the tip prevents it from entering surface recesses below a certain size. Consequently, the topographic images are not faithful projections of the actual film surface but rather a convolution of that function with an appropriate tip function. It remains to be shown, therefore, under what circumstances one can extract accurate fractal dimensions from such topographic images.

Increasing the image resolution to $(1024)^2$ pixel points increases the reliable scaling range to almost two orders of magnitude. However, at this level of resolution each image file is about 4 Mbytes in size making manipulation of data cumbersome. Although it is possible (and desirable) to collect even larger images and use more powerful computers to process them, this solution engenders other problems. Even at optimum piezoelectric raster rates $(1024)^2$ images take approximately half an hour to collect. Increasing this even by a small factor leads to difficulties in maintaining apparatus stability, especially when the sample is cold. We show, however, that reliable results can be obtained with $(1024)^2$ images, the size we use in this study.

Three methods were used to determine the fractal dimension D from our topographic STM images of the deposited Ag films: (i) cube counting,[18] (ii) triangulation,[18] and (iii) power spectrum analysis.[19] In applying the cube counting and triangulation methods, the range of the tip excursions normal to the substrate surface, the z direction, are scaled so that the interval between the lowest and the highest values of z (denoted as capital Z) in the scaled image equals the x or the y range, which are denoted, respectively, X and Y. (In the many images recorded Z was 10–25 % of X or Y for rough films, 3–10 % of X or Y for smooth films, and 6–23 % of X or Y for annealed smooth films.) We will show below that z scaling is essential in obtaining meaningful data from the fractal analysis. Additionally, the area units that will be used in the various log-log plots involving area refer to images that are z scaled as indicated above. Throughout the paper log refers to $\log_{10}$.

(i) In cube counting a cubic lattice with lattice constant L is superimposed on the z-expanded surface. Initially L is set at $X/4$, resulting in a lattice of $4\times4\times4=64$ cubes. All cubes that contain at least one pixel of the image are added and the surface area determined as the total number of such cubes multiplied by L^2. L is then reduced stepwise by factors of 2 and the process repeated until L is equal to two adjacent pixels. The slope of the linear portion of a plot of log(area) versus log(L) gives D directly.

(ii) The algorithm of the triangulation method is similar. Again Z is chosen to equal the X and Y ranges. A grid of unit dimension L is placed on the surface. This defines the location of the vertices of a number of triangles. When $L=X/4$, for example, the surface is covered by 32 triangles of different areas inclined at various angles with respect to the x-y plane. The triangle size, which will be used as a variable in the following analyses, is defined as the length of the projection of triangle sides onto the x-y plane; this is identical to the grid size L. The areas of all triangles are calculated and summed to arrive at the approximant of the surface area corresponding to L. The grid size is then decreased by successive factors of 2, as before, and the process continued until L is two adjacent pixel points. The slope of the resulting log-log plot is $2-D$.

(iii) In the power spectrum method each of the 1024 line height profiles that form the image (each consisting of 1024 points) is Fourier transformed and the power spectrum evaluated. The 1024 power spectra are averaged and the average integrated from high to low frequency. The slope of a log-log plot of this integral versus L^{-1} is $2D-4$.

RESULTS AND DISCUSSION

STM topographic images of the three types of films studied are quite diverse in appearance (Fig. 1). The top three panels of Fig. 1 are $(1\ \mu\text{m})^2$ images; the bottom three are $(200\ \text{nm})^2$ expansions that better depict the detailed morphology of the surface. Figure 1(a) illustrates the granular character of a rough film deposited at 100 K. At the smallest size scale one sees some tip artifacts, i.e., partial images of the tip made visible by surface features of very small size and aspect ratio. The presence of tip artifacts, a ubiquitous feature in STM images of rough surfaces, does not seriously interfere with our fractal analysis. It merely shifts the lower size limit of our images a little upward. (Occasionally more severe artifacts were encountered when the tip was not optimal or when it became contaminated. Such cases were easy to identify and those images were rejected). A higher magnification image of this surface [Fig. 1(b)] shows a cauliflowerlike surface composed of roughness features of all size down to features as small as several nanometers. The smallest florets are spheroidal with dimensions in the range 5–30 nm.

Because the images are topographs of the actual surface one must resist drawing conclusions regarding the three-dimensional structure of the film. Nevertheless, the images shown in Figs. 1(a) and 1(b) are not consistent with the flat grain structure proposed in Ref. 3. They are consistent with the coral-like structure that is expected to arise from aggregation of atoms condensing on the surface with restricted mobility.

Images of smooth Ag films [Figs. 1(c) and 1(d)] show features that are considerably larger than those of the rough Ag films, ranging from 50 to 100 nm in size. A definite structure appears even in the large domain image of Fig. 1(c). The two vertical lines that appear in the image undoubtedly reflect the underlying, mechanically polished Cu surface on which the films were grown. These do not affect our results. A comparison of Figs. 1(b) and 1(d) shows that smooth films lack the variability of size found in the cauliflowerlike surface structure of the rough films.

Smooth Ag films annealed at 560 K for 5 h then cooled back down to 300 K are found to be smoother still. STM images of these annealed smooth films are shown in Figs. 1(e) and 1(f). The average grain sizes are even larger than those for 300 K films.

Raman spectra were attempted for adsorbed benzene and ethylene. Only the rough films showed SERS activity (and indeed very good SERS activity). This is consistent with the notion that SERS results ultimately from the excitation of localized, dipolar surface plasmons, a minimum requirement of which is the presence of metal features with dimensions much smaller than the wavelength of the exciting light. Only the 100 K films satisfy this requirement.

The fractal character of the rough surfaces is demonstrated in the log-log plot (Fig. 2) generated on the basis of cube counting. Results for two different regions of a rough surface are shown in Fig. 2(a); both cover a (100 nm)^2 domain. The linear (scaling) region extends from 0.4 to 25 nm, outside of which the line drops off rapidly as it approaches the digital limits. The persistence of fractal character in rough surfaces up to a critical length scale L_c, beyond which the surface behaves as a homogeneous rather than self-affine object, is well documented.[20] The critical scaling length L_c, which is sometimes written as ξ, can be viewed as a measure of the lateral correlation length for the self-affine surface.[20] L_c was found to lie in the range 25–100 nm for all of the rough surfaces examined in this study. The slopes of the linear portions of the curves shown in Fig. 2(a) produce similar local fractal dimensions $D=2.34$ and 2.39 for the two areas of the rough surface analyzed. The variation in the value of D represents both the effect of error as well as the fluctuation of the value of D across the rough surface.

Figure 2(b) shows data analogous to those in Fig. 2(a) but for a region of the surface 100 times larger in geometric area, spanning (1 μm)^2. Only the linear scaling region is shown. (All subsequent log-log plots will be displayed in this truncated form.) An unrestricted fit to the data shown in Fig. 2(b) yields $D=2.51$, considerably higher than the previously determined value. An examination of Fig. 2(b) indicates, however, that the points are not randomly dispersed about the line. Moreover, an analysis of images of intermediate domain sizes (200 nm)^2 and (500 nm)^2 yields D values consistent with the values of Fig. 2(a) rather than the value 2.51. Here again scaling

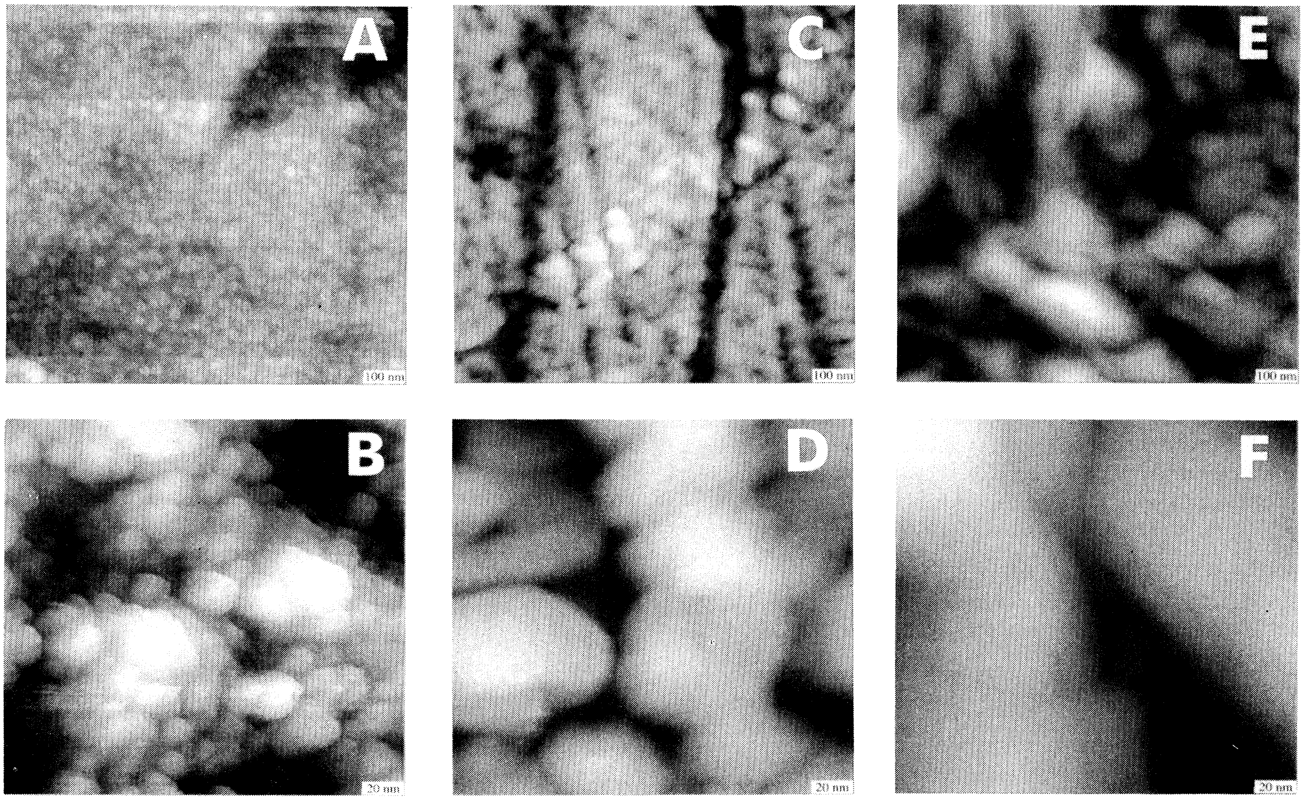

FIG. 1. Constant current topographs of (a) and (b) rough films deposited and imaged at 100 K, (c) and (d) smooth films deposited and imaged at 300 K, and (e) and (f) annealed smooth films deposited at 300 K, annealed at 560 K, and imaged at 300 K. Image domains are (1 μm)^2 for the upper three panels and (200 nm)^2 for the bottom three.

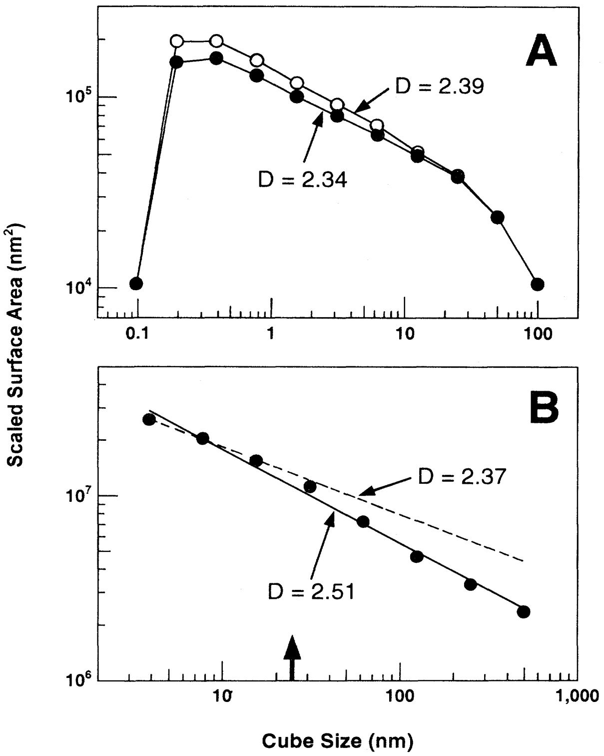

FIG. 2. log-log plots for rough (100 K) Ag films. Cube counting was used to calculate the scaled surface area: (a) (100 nm)^2 domain; (b) (1 μm)^2 domain. The dashed line in (b) is a linear fit to the first three points.

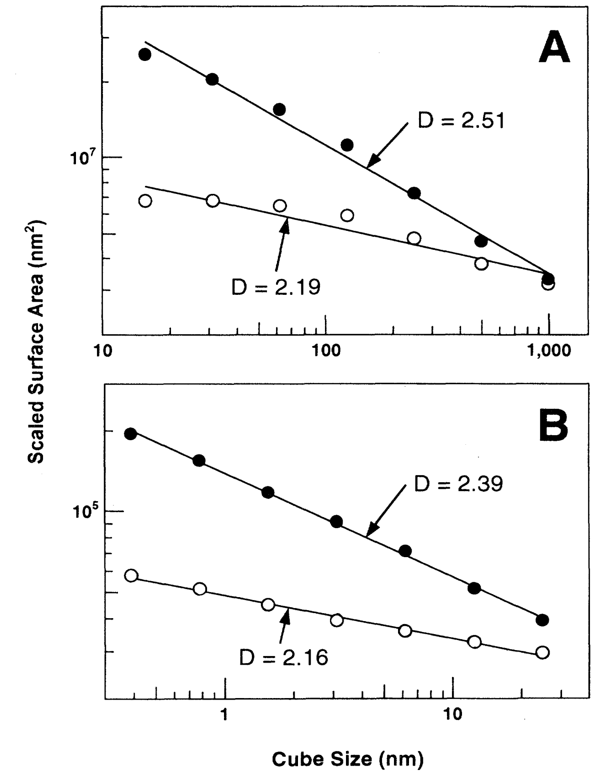

FIG. 3. Comparison of the log-log plots of rough 100 K (filled circles) and smooth 300 K (open circles) Ag films determined by cube counting: (a) (1 μm)^2 domain; (b) (100 nm)^2 domain.

persists only up to approximately 25 nm. The value of D obtained by fitting only the initial portion of Fig. 2(b) is 2.37, in close agreement with the average value of $D = 2.36$ calculated from all of the other images of rough surfaces. This average, along with a measure of the statistical spread, is listed in Table I. The relatively small image-to-image spread in the value of D shows it to be independent of the size of the surface domain investigated as required for a fractal object.

log-log plots of rough and smooth surfaces are compared in Fig. 3. The slopes of the lines for smooth films, and hence the fractal dimension associated with the smooth films (to the extent that the surface is a fractal at all), are significantly lower than those for the rough film, approaching the value corresponding to a nonfractal surface. A most compelling demonstration of the different fractal character of rough and smooth films is possible because of the comparative nature of our data: we are able to investigate the fractality of a rough film contrasted against a background smooth film, with both images collected in the same experiment and with the same tip.

TABLE I. Local fractal dimension of vapor-deposited Ag films. Numerical entries in parentheses are uncertainties in the last significant figure.

Method	Rough films	Smooth films	Annealed smooth films
Cube counting	2.36(3)	2.15(1)	2.11(3)
Triangulation	2.47(5)	2.14(5)	2.06(2)
Power spectrum	2.53(4)	2.56(6)	2.48(2)
Estimated D	2.5	2.1	2.05

Figures 3(a) and 3(b) compare the images obtained by scanning a large (1 μm)^2 and a small (100 nm)^2 area, respectively. Note that in Fig. 3(a) a slight positive curvature appears for both rough and smooth films. This curvature disappears in the smaller domain traces of Fig. 3(b) where the points lie below a cube size of 25 nm. The average value for the local fractal dimension of smooth films is found to be 2.15. This average was calculated from the same number of images and image domain sizes as used to determine D for rough films (Table I).

Annealed smooth films were also imaged. They show characteristics similar to those of smooth films, except that the linear parts of the log-log plots have even smaller slopes. The plots again showed a break in slope at approximately 25 nm.

The triangulation method of analysis produces similar values of D to those obtained with cube counting for images of rough films. Figure 4 shows a series of log-log plots obtained by analyzing data from images of the same rough film, but for increasing domain size. Because the domain sizes of traces A and D in Fig. 4 differ by a factor of 100, the area calculated for any given triangle size should, ideally, differ by that factor. It does not because

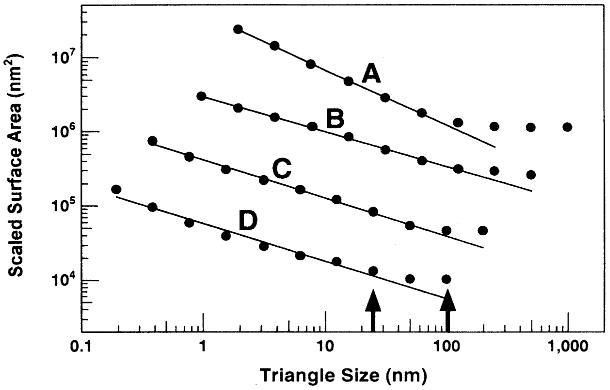

FIG. 4. log-log plots for rough (100 K) Ag films determined by triangulation: A, (1 μm)^2 domain, $D=2.75$; B, (500 nm)^2 domain, $D=2.47$; C, (200 nm)^2 domain, $D=2.51$; D, (100 nm)^2 domain, $D=2.50$.

of the fact that the local fractal dimension is not constant across the film. It is also partly a reflection of the artifacts introduced by this method of analysis. The scaling regions for the log-log plots shown in Fig. 4 terminate at 25–100 nm (marked by the two arrows) according to the scan domain size. In the case of smooth and annealed smooth surfaces the linear portions of the log-log plots obtained by triangulation are even more restricted than those obtained by cube counting (Fig. 5). Plots obtained from images in which large domains were scanned reproducibly show precipitous changes in slope at a triangle size approximately equal to 25 nm.

The upswing in slope observed in Fig. 5(b) (filled circles) at small triangle size is an artifact induced by noise spikes in the STM image data. It is only apparent in small domain scans and it is dramatically reduced if the STM image data are passed through a simple numerical filter before processing [Fig. 5(b), open triangles]. The filter reduces the value of lone pixels, whose brightness values are very different from those of its neighbors, to the average brightness value of neighboring pixels. Smoothing the filtered data [Fig. 5(b), open circles] increases the scaling region further without significantly altering the appearance of the images. The smoothing routine consists of replacing every pixel (not just spikes) in the image by a weighted average of its eight nearest neighbors. Also, the resultant volume under a smoothed region of the surface is normalized so that it is equal to the volume in the raw image corresponding to the same projected area. Use of the numerical filter or the smoothing routine does not change the value of the local dimension: $D=2.09$ for all three traces in Fig. 5(b).

The main features of the results of analyzing the STM images of the same surfaces by power spectrum analysis are summarized in Fig. 6. Results obtained by analyzing small domain images of rough and smooth films are shown in the upper two panels [Figs. 6(a) and 6(c)]. The log-log plots include linear portions exceeding one order of magnitude in size for both cases. However, the local dimensions calculated from these linear portions are almost equal: $D=2.52$ for rough films and $D=2.47$ for smooth films. Results obtained by analyzing large domain images using power spectrum analysis are plotted in Figs. 6(b) and 6(d). These show even more complicated trends including at least two linear portions corresponding to two, sometime quite different, local fractal dimensions. Moreover, the forms of the log-log plots are quite different for rough and smooth films. For log-log plots with more than one linear portion, the robust value of D was assumed to be the one that corresponded to the unique value of D obtained from images of smaller overall size. Equally complicated log-log plots have been reported for data obtained from the STM images of fracture surfaces analyzed by power spectrum analysis.[19] Breaks in the power spectrum analysis of Fig. 6 also occur at approximately $L=25$ nm.

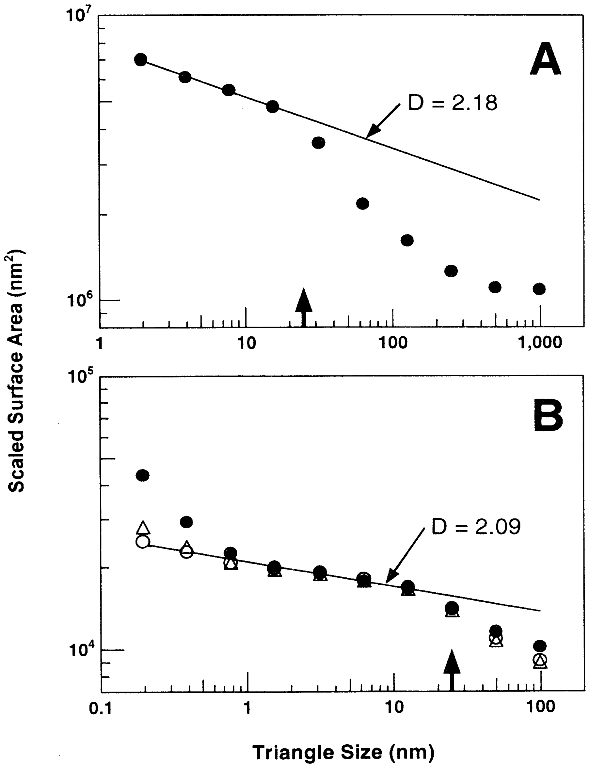

FIG. 5. log-log plots of smooth (300 K) Ag films by the triangulation method: (a) (1 μm)^2 domain; (b) (100 nm)^2 domain. Open triangles are for filtered data; open circles are for filtered and smoothed data.

Table I summarized the values of the local fractal dimensions obtained for the three types of films studied and analyzed by the three methods. For rough films, the values of D determined by the three methods are distributed over a range that exceeds random error. However, they are all in the approximate range 2.4–2.5. In contrast, for smooth and annealed smooth films the three values span a very large range: while cube counting and triangulation produce rather consistent (and small) values, power spectrum analysis returns values of D that are much larger.

The three methods used to determine D should be asymptotically equivalent. The discrepancies arise from the finite size of computed fractal surfaces and the finite

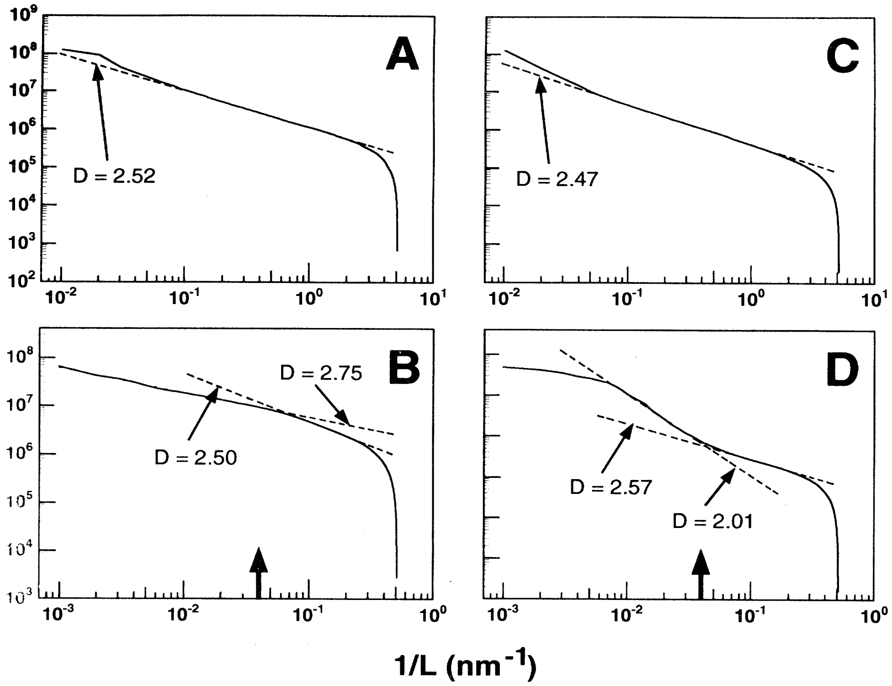

FIG. 6. log-log plots obtained with the power spectrum analysis method: (a) rough (100 K) film, (100 nm)^2 domain; (b) rough (100 K) film, (1 μm)^2 domain; (c) smooth (300 K) film, (100 nm)^2 domain; (d) smooth (300 K) film, (1 μm)^2 domain.

number of points in the images. These deviations should be most profound in systems that have a low degree of fractality. The extent to which these effects influence the value of the fractal dimension was explored computationally by generating various fractal surfaces of known dimension. This was done using the procedure of Voss[21] as described in Ref. 18. The algorithm consists of a random addition of heights to points on a surface grid and of height averaging between neighboring pixel points; the heights are obtained from a normal distribution whose width is given by $\sigma^2(k)=(2^{-1/2})^{k(6-2D)}$, where k is the iteration number. With increasing iteration number the normal distribution width decreases at a rate that reflects the extent of fractality. The initial grid consists of a similar number of pixels as in the experimentally generated topographs. [For computational reasons $(1025)^2$ pixels were used compared to $(1024)^2$ pixels of the experimental topographs.] The fractal dimensions of these computed images were then determined using the three techniques discussed above. The results of this calculation are summarized in Fig. 7, in which the three values of the fractal dimension D(measured), obtained by using cube counting, triangulation, and power spectrum analysis, are plotted as a function of the fractal dimension D(input) assumed in generating the surface.

Ideally the points should all lie on the diagonal line in Fig. 7. The fact that the three methods return different values of D, and specifically that for surfaces with very small fractal dimensions the power spectrum analysis method returns unusually high values of D, clearly indicates that the discrepancy between the true and the apparent fractal dimension obtained by analyzing topographic images is a reproducible characteristic of the methods of analysis for images, the size range, and the number of pixels used in this study. Interestingly, all three methods produce fairly acceptable values of D when D is in the neighborhood of 2.5. Previously it was suggested that the analysis of STM topographic images of fractal surfaces by the power spectrum analysis method produces reliable results provided the images contain at least $(1024)^2$ pixels.[11] We see from Fig. 7 that this condition is not sufficient, although a favorable result for D might be obtained fortuitously if D is between 2.5 and 2.7.

The data shown in Fig. 7 may be used to extract much more accurate values of D of real surfaces from the values of D calculated using the three methods discussed above

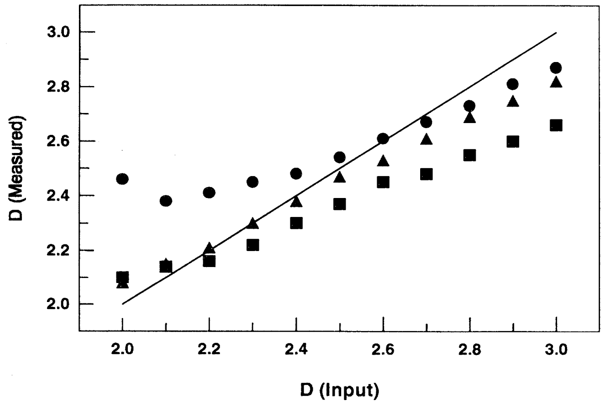

FIG. 7. Comparison of the local fractal dimension D(measured), calculated for numerically generated fractal surfaces as a function of D(input), the fractal dimension assumed in the simulation. Circles refer to the values of D calculated using power spectrum analysis, triangles to triangulation, and squares to cube counting.

provided the behavior shown in Fig. 7 is independent of the particular structure of the fractal surface used to generate it. Indeed, the triplet of points in Fig. 7 corresponding to any given input value of D maps uniquely onto that value. This means that if one determines the three values of D using the three above algorithms then, by using Fig. 7 as a calibration curve, a value of D may be determined from the triplet of points, which is limited by experimental rather than systematic error. (Actually one could deduce the correct fractal dimension from either of the calibration curves obtained with cube counting and triangulation. The redundancy of using all three improves the confidence with which the value is determined.) Using this technique we were able to estimate trustworthy fractal dimensions for the three surfaces studied. These are listed in Table I. These values imply that only the films prepared at 100 K are fractal. Films prepared at 300 K retain some vestiges of fractality, but are largely nonfractal. Films deposited at 300 K and annealed at 560 K are nonfractal.

One should mention parenthetically that surfaces of Ag films deposited at 100 K then subsequently annealed to 560 K were also imaged. Intriguingly, the resulting surfaces were extremely smooth—smoother than the surfaces of films deposited at 300 K and then annealed—often showing large $[>(200\ \mathrm{nm})^2]$ single crystal faces. This suggests that the dynamic processes responsible for annealing are sensitive to the film's initial structure.

The need to expand z so that the range of z corresponds to (or exceeds) the ranges of x and y results from both the limited x and y ranges and the limited image resolution inherent in the experiments, which in turn restricts the range of values that L can have. This is demonstrated in the Appendix. The effect of z scaling is also illustrated in Fig. 8 where the value of D calculated by triangulation from a generated fractal surface with $D(\text{input})=2.5$ is plotted against the z-scaling factor. The surface was generated such that the range of z was equal to the range of x and y so that X/Z (and Y/Z)$=1$. The range of z was then scaled by a factor M^{-1} such that M was both greater than and less than unity. ($M<1$ implies that Z exceeds X and Y.) Figure 8 shows that with M equal to 1 the slope of the log-log plot corresponds closely to $D=2.5$, the input value. When M increases beyond 1 the calculated value of D quickly decreases to the trivial value $D=2$, while for $M<1$, fairly constant values of D close to $D=2.5$ are obtained. All the calculations we have performed on the STM images have been checked in the context of z scaling so that the D values quoted are the best values of the local dimension.

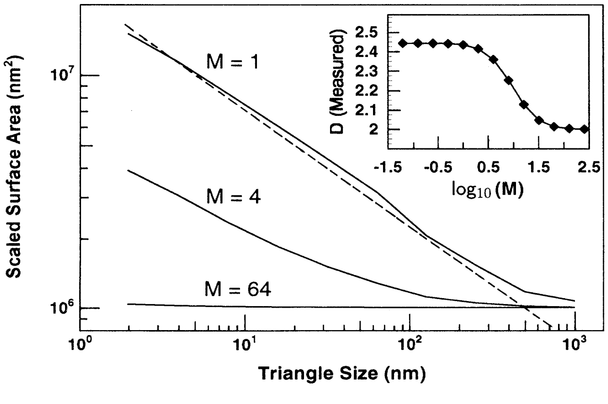

FIG. 8. log-log plot of a generated fractal surface ($D=2.5$) by triangulation. M is the z-axis scaling ratio $M=X/Z=Y/Z$. The dashed line represents the theoretical slope for $D=2.5$.

A question that must still be resolved is the degree to which the apparent value of D determined is altered by the fact that the measured topographs are convolutions of the surface structure with that of the tip. Clearly topographic details of small crevices are severely distorted in the STM images as a result of the tip's inability to enter small recesses. Although it is unclear precisely below what size this problem becomes unacceptably severe, it is clear that by recording images of sufficient range and resolution one should have enough data in the image beyond this lowest size limit from which reliable fractal dimensions may be determined. Even above this lower-dimensional bound one is measuring a structural average produced by tunneling to an extended portion of the tip rather than to a point. Fortunately, the scaling property of fractals ensures that the fractal dimension determined will be independent of such averaging. We believe that, with the range and resolution used in our study, the fractal dimensions determined for the rough films represent accurately the structure of their surfaces.

Fractality is a statement of the fact that a particular structure has dilation symmetry. Knowledge of the fractal dimension does not, in general, convey any other morphological information regarding the system. Systems that are very different morphologically can be characterized by the same fractal dimension and vice versa. Nevertheless, the fractal dimension can sometimes be used to exclude certain structural or dynamical possibilities. For example, colloidal particle assemblies that form in solution by cluster-cluster aggregation are fractals characterized by a fractal dimension approximately equal to 1.75, while those that form by diffusion-limited aggregation have much larger fractal dimensions.[22]

The scaling properties of rough surfaces have been studied extensively.[20(a)] A number of continuum equations have been proposed to simulate the growth of rough surfaces through processes that include stochastic deposition or dissolution. These have been reviewed recently.[20(a)] The fractal dimension of the self-affine surfaces generated by these continuum equations range from 2 to 3. On the basis of our measured value of $D\sim2.5$ we can reject certain growth mechanisms as the dominant ones in forming the surfaces. Specifically the surfaces do not form by simple stochastic roughening, which is characterized by a value of $L_c=0$. Values of $D\sim2.5$ are not uncommon for rough surfaces formed by deposition or erosion. Fe films roughened by Ar^+ bombardment are also found to be self-affine with $D\sim2.5$.[15]

Our STM images contain far more morphological information than that summarized in the fractal dimension. In particular, they show that Ag films formed by condensation of atomic vapor onto a low-temperature substrate under the deposition conditions that we use are not flat mesas separated by narrow crevices as proposed in Ref. 3. And although a detailed picture of the film structure cannot be determined from the STM topographic images, the results are consistent with the coral-like structures discussed in Ref. 5. Our results also strongly suggest that SERS is largely a phenomenon related to the excitation of dipolar localized surface plasmons. Surfaces that show strong SERS were found to be composed of closely interacting structures with individual dimensions much smaller than the wavelength, hence structures that can sustain dipolar localized plasmon excitations. Surfaces that were composed of features of the order of, or larger than, the wavelength did not produce SERS. Although we believe that for a system to show strong SERS it must consist of an assembly of particles or structures that are coupled, it is not necessary that the assembly be fractal for it to be SERS active. If it is, however, then one can test the predictions regarding the response of fractal clusters to optical fields.[7(a)] These theories[7(b),7(c)] hold out the promise that certain aspects of SERS (as well as of other optical effects) observed on fractal systems may be understood quantitatively to a degree that is, in general, impossible to achieve for disordered systems, which are non-fractal.

CONCLUSIONS

Ag films were prepared by condensing Ag vapor onto a support held at 100 or 300 K and STM images were obtained at the deposition temperatures. Additionally, images of Ag films deposited at 300 K, then annealed at 560 K, and imaged at 300 K were also obtained. An analysis of the scaling properties of the topographic images suggests that films deposited at 100 K are self-affine with local Hausdorff-Besicovitch dimension $D=2.5$. SERS activity has been confirmed for these films in the same experiment. Films deposited at higher temperature possess relatively little fractality and no SERS activity. We also show that systematically erroneous fractal dimensions may be produced by certain algorithms for determining the fractal dimension even with large scans at resolutions characteristic of current STM technology. However, much more accurate values of D may be determined by combining the results obtained from several algorithms with a calibration curve generated by applying the same algorithms to simulated fractal surfaces of known Hausdorff-Besicovitch dimension.

ACKNOWLEDGMENTS

The authors are grateful to Dr. Vladimir Shalaev for many exciting discussions. Funding from NSERC and CEMAID is gratefully acknowledged.

APPENDIX

We will demonstrate that the fractal dimension obtained from a surface approaches its correct limit asymptotically only when the range spanned by the direction normal to the projected surface, the z dimension, is expanded to correspond to or exceed the ranges of the plane of the surface. The demonstration is most easily performed for a fractal line rather than for a surface. The case of the surface follows directly.

The analog to the triangulation method for a fractal line involves dividing the two-dimensional space containing the line into N equal segments of width L. An approximant to the length of the line is given by the sum of the straight-line segments defined by the intercepts of the fractal line with the set of parallel lines defining the N segments. The length l of the approximant corresponding to segments of width L is given by

$$l=\sum_{i=1}^{N}[(z_i-z_{i+1})^2+(x_i-x_{i+1})^2]^{1/2}\ , \tag{A1}$$

i.e.,

$$l=\sum_{i=1}^{N}[(\delta z_i)^2+L^2]^{1/2}\ . \tag{A2}$$

If the z dimension is scaled by a constant M^{-1}, then the expression for l becomes

$$l=\sum_{i=1}^{N}[(\delta z_i)^2/M^2+L^2]^{1/2}\ . \tag{A3}$$

The fractal dimension is normally obtained from the slope of the function $\log_{10}(l)$ vs $\log_{10}(L)$. The range of L spans the limits $L_{\max}$ to $L_{\min}$, so that the mean value of L contributing significantly to the plot is of the order of $L_{\max}$. Consequently, if most of the $(\delta z_i)^2/M^2$ terms in Eq. (A3) are smaller than $L_{\max}^2$, then l, as given by Eq. (A3), will be dominated by the L terms and l will scale trivially as L^1. By choosing values of M that are small enough one ensures that the expression for l contains sufficient nontrivial z terms to produce a meaningful value of D. If the largest values of $|\delta z_i|$ are inherently of the order of $L_{\max}$, then the switch from the condition in which Eq. (3) produces trivial values of D, to that in which it contains meaningful information regarding D, will occur when M is of the order of unity.

---

[1] D. L. Jeanmarie and R. P. Van Duyne, J. Electroanal. Chem. **84**, 1 (1977); M. G. Albrecht and J. A. Creighton, J. Am. Chem. Soc. **99**, 5215 (1977); M. Fleischmann, P. J. Hendra, and A. J. McQuillan, Chem. Phys. Lett. **26**, 163 (1974).

[2] M. Moskovits, Rev. Mod. Phys. **57**, 783 (1985), and references therein.

[3] E. V. Albano, S. Daiser, R. Miranda, and K. Wandelt, Surf. Sci. **150**, 367 (1985); **150**, 386 (1985), and references therein.

[4] J. K. Gimzewski and A. Humbert, IBM J. Res. Dev. **30**, 472 (1986).

[5] G. S. Bales, R. Bruinsma, E. A. Eklund, R. P. U. Karunasiri, J. Rudnick, and A. Zangwill, Science **249**, 264 (1990).

[6] J. T. Stuckless and M. Moskovits, Phys. Rev. B **40**, 9997 (1989).

[7] (a) M. I. Stockman, V. M. Shalaev, M. Moskovits, R. Botet, and T. F. George, Phys. Rev. B **46**, 2821 (1992); (b) V. A. Markel, L. S. Muratov, M. I. Stockman, and T. F. George, *ibid.* **43**, 8183 (1991); (c) M. I. Stockman, T. F. George, and V. M. Shalaev, *ibid.* **44**, 115 (1991).

[8] A. V. Butenko, P. A. Chubakov, Yu. E. Danilova, S. V. Karpov, A. K. Popov, S. G. Rautian, V. P. Safonov, V. V. Slabko, V. M. Shalaev, and M. I. Stockman, Z. Phys. D **17**, 283 (1990).

[9] C. Douketis, T. L. Haslett, J. T. Stuckless, M. Moskovits, and V. M. Shalaev, Surf. Sci. Lett. **297**, L8 (1993); V. M. Shalaev, C. Douketis, and M. Moskovits (unpublished).

[10] R. Chiarello, V. Panella, and J. Krim, Phys. Rev. Lett. **67**, 3408 (1991).

[11] M. W. Mitchell and D. A. Bonnell, J. Mater. Res. **5**, 2244 (1990).

[12] K. Sakamaki, K. Itoh, A. Fujishima, and Y. Gohshi, J. Vac. Sci. Technol. A **8**, 525 (1990).

[13] D. R. Denley, J. Vac. Sci. Technol. A **8**, 603 (1990).

[14] J. M. Gomez-Rodriguez, A. M. Baro, and R. C. Salvarezza, J. Vac. Sci. Technol. B **9**, 495 (1991).

[15] J. Krim, I. Heyraert, C. Van Haesendonck, and Y. Bruynseraede, Phys. Rev. Lett. **70**, 57 (1993).

[16] C. Douketis, V. M. Shalaev, T. L. Haslett, Z. Wang, and M. Moskovits, J. Electron Spectrosc. Relat. Phenom. **64/65**, 167 (1993); Physica A **207**, 352 (1994).

[17] R. L. Summers, NASA Technical Report No. D-5285, Washington, DC, 1969 (unpublished).

[18] J. Feder, *Fractals* (Plenum, New York, 1988), and references therein.

[19] B. B. Mandelbrot, D. E. Passoja, and A. J. Paullay, Nature **308**, 721 (1984).

[20] (a) W. M. Tong and R. S. Williams, Annu. Rev. Phys. Chem. **45**, 401 (1994); (b) E. Courtens, R. Vacher, J. Pelous, and T. Woignier, Europhys. Lett. **6**, 245 (1988); R. Vacher, T. Woignier, J. Pelous, and E. Courtens, Phys. Rev. B **37**, 6500 (1988); R. Vacher, E. Courtens, E. Stoll, M. Böffgen, and H. Rothuizen, J. Phys.: Condens. Matter **3**, 6531 (1991); E. P. Stoll and M. Kolb, Physica A **185**, 222 (1992).

[21] R. F. Voss, in *Fundamental Algorithms in Computer Graphics,* edited by R. A. Earnshaw (Springer-Verlag, Berlin, 1985); also see J. Feder, *Fractals* (Ref. 18), pp. 221–228.

[22] D. A. Weitz and M. Olivera, Phys. Rev. Lett. **52**, 1433 (1984); D. A. Weitz, M. Y. Lin, J. S. Huang, T. A. Witten, S. K. Sinha, J. S. Gertner, and C. Ball, in *Scaling Phenomena in Disordered Systems,* edited by R. Pynn and A. Skjeltorp (Plenum, New York, 1985), pp. 171–188.

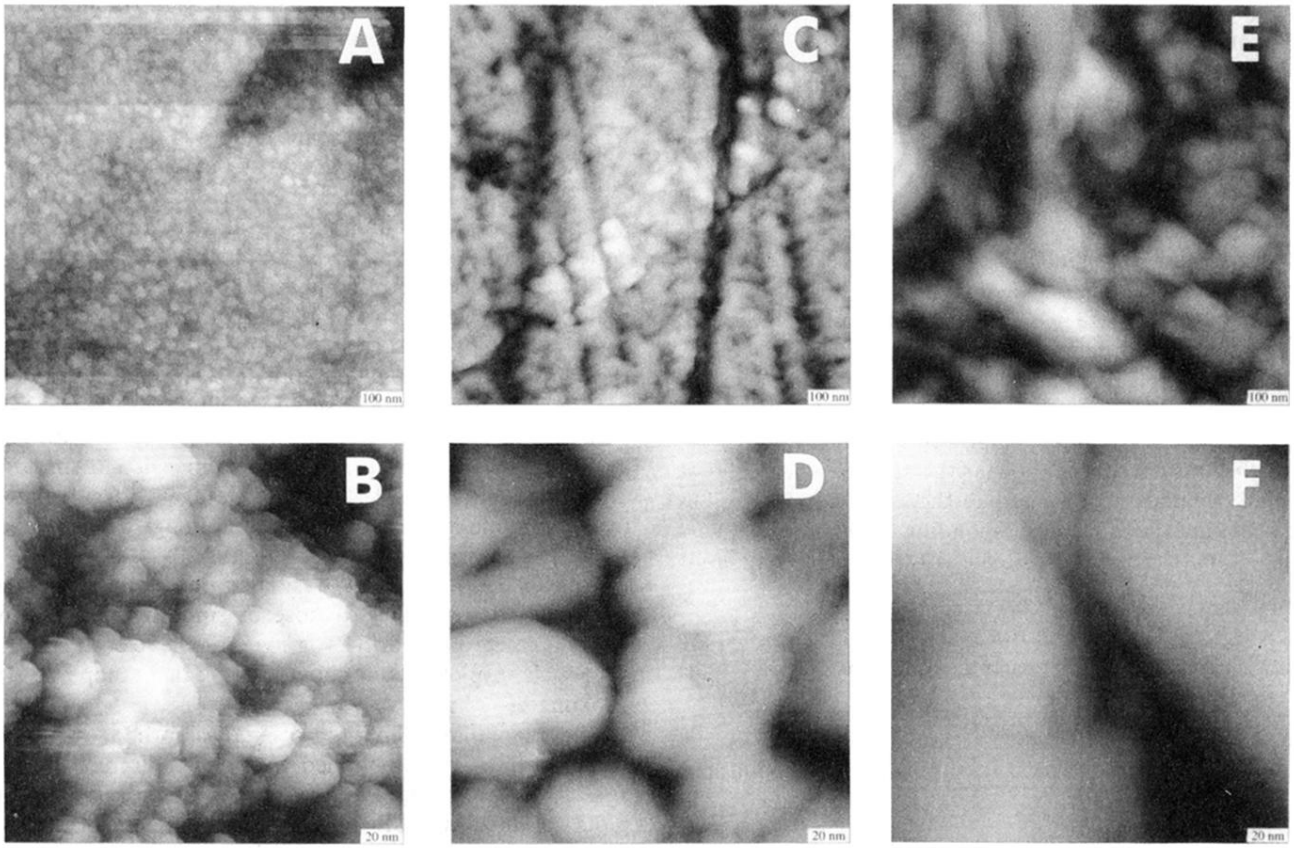

FIG. 1. Constant current topographs of (a) and (b) rough films deposited and imaged at 100 K, (c) and (d) smooth films deposited and imaged at 300 K, and (e) and (f) annealed smooth films deposited at 300 K, annealed at 560 K, and imaged at 300 K. Image domains are $(1\ \mu\mathrm{m})^2$ for the upper three panels and $(200\ \mathrm{nm})^2$ for the bottom three.